ProteinMPNN-based Backbone Redesign and Conformational Biasing to Increase Membrane Targeting and Conductance of a Chimeric Ion Channel

Simon Pritchard [1 2 3]

Abstract

Here we apply to ProteinMPNN-based techniques for protein engineering. First recapitulating the results from *Dauparas et al.*, we perform additional ablations to verify the functionality of the ProteinMPNN architecture. We then use ProteinMPNN to generate backbone redesigns for improved stability to improve membrane-targeting, as well as using conformational biasing (Cavanagh et al., 2025) to increase the conductance of the MAGIC system. Most mutants are ultimately deleterious in function, but marginal increases in membrane-targeting are achieved using the backbone redesign.

1. Introduction

Inverse folding of proteins has revolutionized tool development in creating high-fidelity backbones that confer extreme stability — often more than endogenous. The most widely used model to do so is ProteinMPNN, an encoder/decoder network that is incredibly effective given its comparably sparse architecture (1.6M parameters). It is able to get away with so few parameters because its inputs are reused time and time again. Upon parsing an input structure, the coordinates are made invariant, node and k-nearest edge features are extracted, and then passed through a 3-layer, 128 dimension encoder module. To get a final protein sequence, the decoder predicts (randomly) for a residue to be assigned. Other residues are masked upon decoding such that the outputs are conditioned only upon the three-dimensional structure itself. The outputs themselves can be compiled to create a distribution for an amino acid at any given sequence position. These log probabilities form the conceptual and mathematical foundation for conformational biasing as developed in (Cavanagh et al., 2025).

1.1. Conformational Design with ProteinMPNN

Conformational Design was born out of necessity to be able to shift dynamic proteins towards a certain conformation required for a design task. Originally developed to increase the activity of lplA, an enzyme, the method has expanded such that it can be applied to almost as diverse a group of protein as any competitor. Conformational biasing achieves this result by 1) generating *n* ProteinMPNN backbone redesigns, 2) computing a distribution for each amino acid/position using the frequency of mutations, scaling and differencing the observed log-probabilities. The larger the difference, the more the mutation favors the allostery of state 1 over state 2.

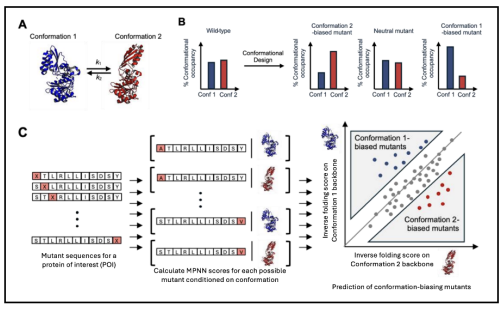

Figure 1. Schematic of conformational design pipeline. **A)** Proteins alter conformations with some rate *k*. **B)** Schema for how point substitutions can alter the relationship between the conformational states to bias the structure in favor of some state. **C)** Conformational design evaluates substitution mutations along the protein sequence and compares MPNN scores conditional on conformational state for biasing mutants. (Cavanagh et al., 2025)

1.2. Modular Antigen-Gated Ion Channels (MAGICs) for Greater Precision in Neuronal Modulation

In this project we aimed to apply both of these inverse-folding techniques, both based on ProteinMPNN to Modular Antigen-Gated Ion Channels (MAGICs), a platform being developed in Dr. Alice Ting's lab for more context-specific perturbation of neural systems. These engineered channels are meant to address the lack of tools for modulat-

[1]Department of Biology, Stanford University [2]Department of Statistics, Stanford University [3]Alice Ting Lab, Department of Genetics, Stanford School of Medicine. Correspondence to: Simon Pritchard <skpritch@stanford.edu>.

Proceedings of the 42^{nd} International Conference on Machine Learning, Vancouver, Canada. PMLR 267, 2025.

ing circuits with connection level specificity — even despite recent advances in programming neuronal activity using optogenetic or chemogenetic methods. MAGICs present a modular, antigen-dependent, chemogenetic platform to drive cellular electrical signals (excitatory or inhibitory) in response to user-defined antigens, with high spatial resolution. The antigen-gating results from fusing a nanobody and an auto-inhibitory peptide to the excitatory or inhibitory LGIC. Binding of connection-specific antigens relieves autoinhibition and enables LGIC activation by a synthetic molecule, PSEM.

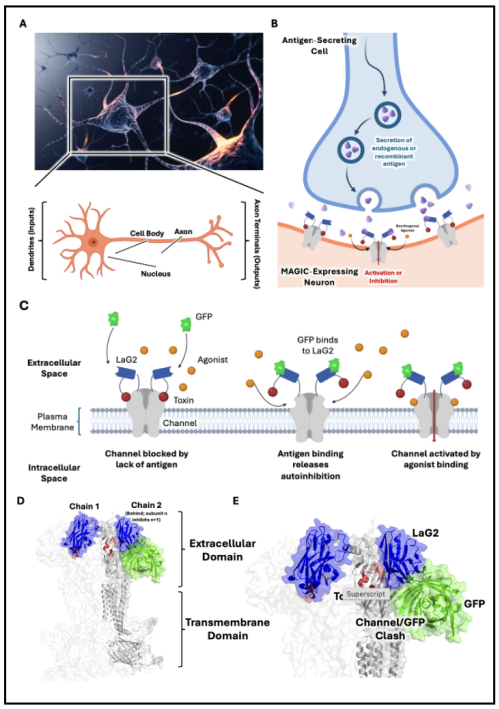

Figure 2. Modular Antigen-Gated Ion Channels (MAGICs) can be used to more precisely perturb neuronal systems. **A)** Neural systems are highly complex with many individual input and output nodes per neuron. **B)** A chimeric channel with activation conditioned on an antigen for activation would add context control for cell behavior modulation. **C)** The biorthogonal channel has an autoinhibitory domain (toxin-based) that prevents activation in the absence of some antigen (i.e GFP). Upon binding, the steric clash removes the autoinhibition and allows for activation by agonist. **D)** MAGICs are based on a biorthogonal homopentamer. **E)** The autoinhibitory domain is made up of an antigen-binding nanobody (i.e LaG2), and a toxic peptide that binds to the ligand-binding pocket. Upon antigen binding a steric clash occurs with the channel.

The two areas of weakness MAGICs currently suffer from include 1) high rates of membrane trafficking, and 2) a decrease in signal transduction from their WT counterparts — due primarily to incomplete release of auto-inhibition upon antigen binding. We hypothesized that 1) we could use ProteinMPNN to do whole-backbone redesigns and substantially increase the stability of the channels. This would, in theory, have the effect of reducing the amount of intracellular trapping due to protein QC. We also decided to apply conformational biasing to all pairs of the three ion channel states — open, desensitized, and closed — to favor the open state over the desensitized state, increasing total conductance (i.e signal transduction) per activation.

2. Reproducing Initial ProteinMPNN Performance

To fully understand inverse-folding before applying it to MAGICs, we re-implemented the ProteinMPNN model. Using the code base from the ProteinMPNN code base (Dauparas et al., 2022), we retrained the model in its entirety using a database of 27k protein structures from the Baker Lab. It is worth noting that we trained all MPNN models on the 2021 split of the dataset, while *Dauparas et al.* made use of the 2020 version.

The first test we performed was to reproduce *Table 1* from *Dauparas et al.*, which illustrates the changes that differing architectures make to ProteinMPNN in terms of sequence recovery and perplexity. In addition to a baseline model (which accepts only Cα's and uses autoregressive decoding), experiment 1 incorporates the additional heavy-atom distances which lend significant accuracy to the model. Experiment 2 incorporates a small MLP to update the edge weights between passes for a given protein. Experiment 3 combines 1 & 2, and also adds random decoding. Together, these modifications to the baseline architecture substantially improve its efficacy. Notably, our re-implemented models perform marginally better (by 2% in sequence recovery, and 0.5 in perplexity). We suspect this is due to training on a newer, higher-quality dataset. As illustrated later, our model training patterns are almost entirely consistent with the original ProteinMPNN supplementary information, so it would be in-line that the increase in testing ability is due to better generalization from building on the training data.

3. MPNN Noise-Robustness and Model Ablations

Beyond our replication of *Table 1*, we also performed several ablations in line with *Dauparas et al.*. We ran a spread to test how differing levels of Gaussian noise for the backbone in training affect perplexity and sequence recovery. As visible in 3A, increasing levels of noise also increase the perplexity (higher perplexity is worse). For σ=0.02, 0.1, 0.2Å, its evident that our training and validation perplexity across epochs is almost identical to that from *Dauparas et al.* in 3B, (note that the red lines in 3A are $\sigma = 0.4$, and in 3B $\sigma = 0.3$. Due to the computational costs of running

Table 1. Replication of Table 1 from *Dauparas et al.* Sequence recovery percentages and test perplexities (exponentiated categorical cross-entropy loss) for models with various modifications. Sequence recoveries and perplexities shown for both re-implementation and the original scores from *Dauparas et al.*

REIMPLEMENTATION / *Dauparas et al.*	MODIFICATION	SEQUENCE RECOVERY (%)	TEST PERPLEXITY
BASELINE	NONE	42.8/40.1	6.64/6.77
EXPERIMENT 1	ADD N, Cα, C, Cβ, O DISTANCES	48.6/46.1	5.43/5.54
EXPERIMENT 2	UPDATE ENCODER EDGES	44.1/42.0	6.28/6.37
EXPERIMENT 3	COMBINE 1 AND 2	49.5/47.3	5.30/5.36
EXPERIMENT 4	EXPERIMENT 3 WITH AGONISTIC DECODING	50.2/47.9	5.21/5.25

inference on large numbers of structures with AlphaFold, this paper solely uses sequence recovery percentages and perplexity to compare models. We performed testing using a set of 300 structures drawn randomly. As expected in testing, increasing levels of Gaussian noise decrease the sequence recovery (lower accurate reconstruction) but increase perplexity (increasing backbone diversity). We also recapitulate the Cα-only model, and similarly as expected, it underperforms in sequence recovery across a spread of Gaussian noise by 6% — consistent with S9A from *Dauparas et al.*. Finally, we perform two more ablations. We test a spread of values for the k-nearest neighbor parameter that dictates the number of edges a single node can relate to, as well as a spread of hidden dimension sizes for the encoder/decoder layers. Predictably, increasing k-nearest neighbors improves model performance, (but at the cost of compute time). Sensibly — given that the final MPNN model uses 48 nearest neighbors — the performance boost above 48 neighbors is minimal. Also as expected, increasing the size of the hidden dimension improves sequence recovery and reduces perplexity.

4. Backbone Redesign for Greater Membrane-Targeting

Since MAGICs are chimeric with significant domains beyond the endogenous channel, AlphaFold3 was used to generate an input structure for ProteinMPNN to predict on. Before running MPNN, 85% of the residues were masked (unavailable for alteration by MPNN). These included the toxin, ligand binding-adjacent residues in the extracellular domain, LaG2, mScarlet, and all residues in the ion pore domain. After 1024 backbone-redesign sequences were generated, ESM2 scores were computed. Sequences were filtered by removing the bottom 75% based on these scores. The remaining 240 sequences were run through

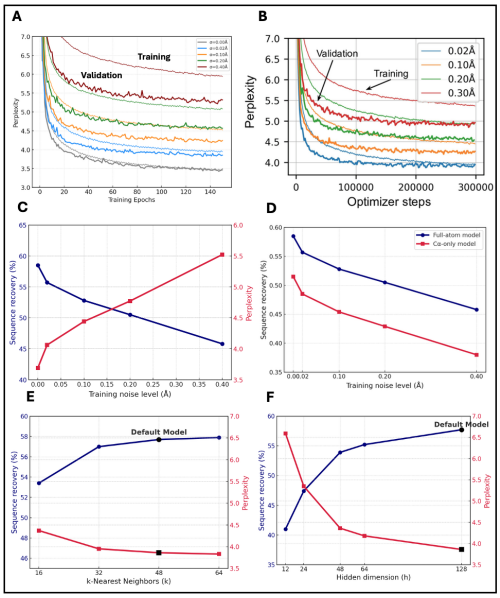

Figure 3. Replication of figures in *Dauparas et al.*, investigating ablations of ProteinMPNN. **A)** Training and validation perplexity across 150 epochs of training. Model improvements begin plateauing after 60 epochs. **B)** Training and validation perplexity across 300,000 optimization steps (Dauparas et al., 2022). **C)** and **D)** Comparisons of sequence recovery and perplexity between the full-atom model and a coarse-grained Cα-only model across a Gaussian noise spread. **E)** and **F)** Examining sequence recovery and perplexity for ablations of the k-nearest neighbors examined by the model and the size of the hidden layers, respectively. Importantly, the metrics for the k-nearest neighbor and hidden dimension ablations are validation rather than test due to time constraints, (perplexity is lower and sequence recovery is higher than it should be).

AlphaFold2 to generate pLDDT and pTM scores. Binning across sequence identity, the top sequence from each bin was selected according to it having the highest product of scaled pLDDT and pTM scores. The 10 most diverse were selected and a subset were tested (Figure 7, S1). Looking across all sequences, the top 12, 60 most common point mutants were also put into designs and tested (Figure 4B). Mutants tended to be concentrated in the flexible linker regions that were suspected to be a source of instability for the channel. For each construct, a membrane potential assay was run to determine whether the channel was still capable of conducting an ionic current upon the addition of an agonist. FACS was also run with MAGIC-expressing cells being incubated with a membrane-impermeable toxin to test the correct construction of channels on the cell surface (a quantitative proxy for membrane targeting). Finally, live-cell imaging was done with the internal mScarlet (in the M3-M4 loop) acting as an expression marker. Overall, there tended to be a marginal increase in membrane trafficking beyond the "WT" sequence. However, it came at the cost

of a loss of functionality. As sequence identity to the "WT" decreased, so did the observed conductance of the channel. While the "Top12" mutant showed full conductance, it lost the antigen dependence integral to the MAGICs's spatial resolution.

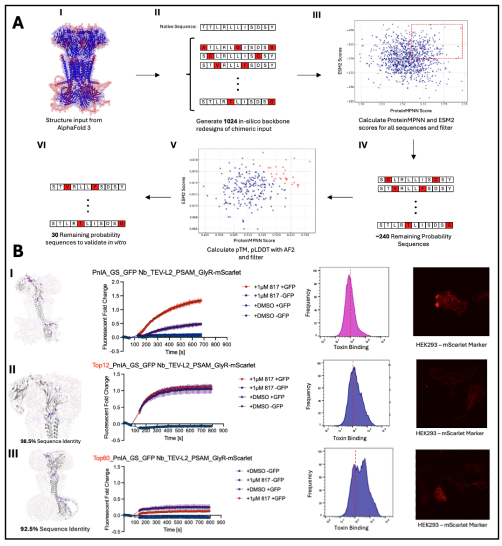

Figure 4. MPNN-based backbone redesign marginally improves membrane targeting at the cost of antigen-dependent conductance. **A)** Filtering design for MPNN-generated backbones. The top 25% are selected based on MPNN and ESM2 scores, 30 scores are selected from the filtered set using AF2-generated pLDDT and pTM scores. **B)** MAGIC structure shown with potential or true mutation sites, MP functionality assay, FACS assay, and live-cell imaging for *(I)* WT inhibitory MAGIC channel, *(II)* backbone with the 12 highest point mutations, *(III)* backbone with the 60 highest point mutations. Top12 was the only redesigned channel that showed full conductance (but lost antigen-dependence). Higher levels of membrane-targeting are evidenced by the FACS results which use a membrane-impermeable toxin to measure surface presentation.

5. Conformational-Bias Redesign for Increased Conductance

To perform conformational biasing across three states, pairwise CB was run (three in total), with the goal of selecting mutations that biased open over desensitized, but did not effect either states' relationship with the closed channel state (Figures 5A, 5B). Finally, each of the top 10 mutants were cloned and run through the membrane potential assay. Similarly to the backbone redesigns, most mutations resulted in a severe LOF. One mutant, L307S, maintained the same level of activation as the "WT" but did not increase total conductance.

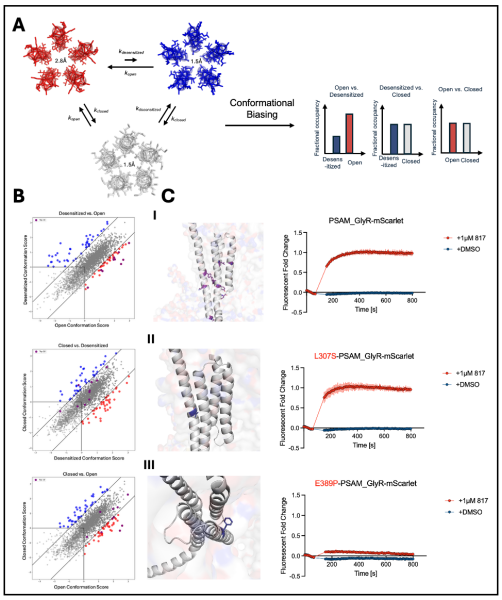

Figure 5. Conformational bias fails to generate channels with higher conductance; most point mutations result in complete loss of function. **A)** Given open, desensitized, and closed channel states we seek to rebalance allostery in favor of the open state over desensitized, but not disrupting either equilibrium with closed. **B)** Scatterplots showing pairwise CB results, 10 selected mutations shown (purple). **C)** IPD with highlighted point mutant, membrane potential assay results for (I)WT chimeric channel, (II) L307S was the highest-functioning mutant, (III) E389P was characteristic of most point mutants selected.

6. Conclusion

While the inverse-folding techniques applied in this paper were by no means ecstatically successful, their working applications throughout the literature continue to imply their usefulness. The ProteinMPNN-based redesigns were successful in increasing membrane presentation, if not as drastically as hoped for — and had a deleterious effect on function.

While one can no doubt improve the filtering pipeline — or perhaps more intense mutant screens — this study emphasizes the complexity of the MAGIC system. The homopentameric nature of the channel, and the complex mechanics that dictate its conductance, present more of a challenge than the majority of applications evidenced in the literature. *Cavanagh et al.*, while a significant and thorough paper, does not investigate multimers with more than two chains for use with conformational biasing. Likewise, the LOF correlated with decreasing sequence identity in the backbone redesigns implies a highly sensitive channel architecture. In future, point mutation screens are likely a superior strategy to swapping out 15% of amino acids simultaneously — even despite the rigorous masking procedure utilized here.

References

Abramson, J., Adler, J., Jumper, J., Hassabis, D., Kelley, D. R., and Silver, D. Accurate structure prediction of biomolecular interactions with *AlphaFold* 3. *Nature*, 630: 493–500, 2024. doi: 10.1038/s41586-024-07487-w.

Cavanagh, P. E., Xue, A. G., Dai, S., Qiang, A., Matsui, T., and Ting, A. Y. Computational design of conformation-biasing mutations to alter protein functions. *bioRxiv*, 2025. doi: 10.1101/2025.05.03.652001. Preprint.

Dauparas, J., Anishchenko, N., Jumper, I., and Baker, D. Robust deep learning–based protein sequence design using ProteinMPNN. *Science*, 378(6614):49–56, 2022. doi: 10.1126/science.add2187.

Evans, S. W., Nguyen, L. N., Atique, J. C., and Lin, M. Z. A positively tuned voltage indicator reveals electrical correlates of calcium activity in the brain. *bioRxiv*, 2021. doi: 10.1101/2021.10.21.465345. Preprint.

Evans, S. W., Sun, J., Fenno, M., and Lin, M. Z. A positively tuned voltage indicator for extended electrical recordings in the brain. *Nature Methods*, 20(7):1104–1113, 2023. doi: 10.1038/s41592-023-01913-z.

Gielen, M., Thompson, A. R., and Smart, T. G. The desensitization gate of inhibitory *Cys*-loop receptors. *Nature Communications*, 6:6829, 2015. doi: 10.1038/ncomms7829.

Kalogriopoulos, N. A., Tei, R., Yan, Y., Klein, P. M., Ravalin, M., Cai, B., Soltesz, I., Li, Y., and Ting, A. Y. Synthetic GPCRs for programmable sensing and control of cell behaviour. *Nature*, 637:230–239, 2024. doi: 10.1038/s41586-024-08282-3.

Kumar, A., Basak, S., Rao, S., Rahman, K., and Gouaux, E. Mechanisms of activation and desensitization of full-length glycine receptor in lipid nanodiscs. *Nature Communications*, 11:3752, 2020. doi: 10.1038/s41467-020-17364-5.

Magnus, C. J., Lee, P. H., Atasoy, D., Su, H. H., Looger, L. L., and Sternson, S. M. Chemical and genetic engineering of selective ion channel–ligand interactions. *Science*, 333(6047):1292–1296, 2011. doi: 10.1126/science.1206606.

Magnus, C. J., Lee, P. H., Bonaventura, J., et al. Ultrapotent chemogenetics for research and potential clinical applications. *Science*, 364:eaav5282, 2019. doi: 10.1126/science.aav5282.

Noviello, C. M., Gharpure, A., Yi, H.-T., Dravid, J., and Hibbs, R. M. Structure and gating mechanism of the α7 nicotinic acetylcholine receptor. *Cell*, 184(8):2121–2134.e13, 2021. doi: 10.1016/j.cell.2021.02.049.

Yu, J., Zhu, H., Lape, R., Greiner, T., Du, J., Lü, W., Sivilotti, L., and Gouaux, E. Mechanism of gating and partial agonist action in the glycine receptor. *Cell*, 184(4):957–968.e21, 2021. doi: 10.1016/j.cell.2021.01.026.

A. Supplementary Figures

The code base used herein can be found at MPNN-Recapitulation. For any questions about specific laboratory methods, please contact the corresponding author.

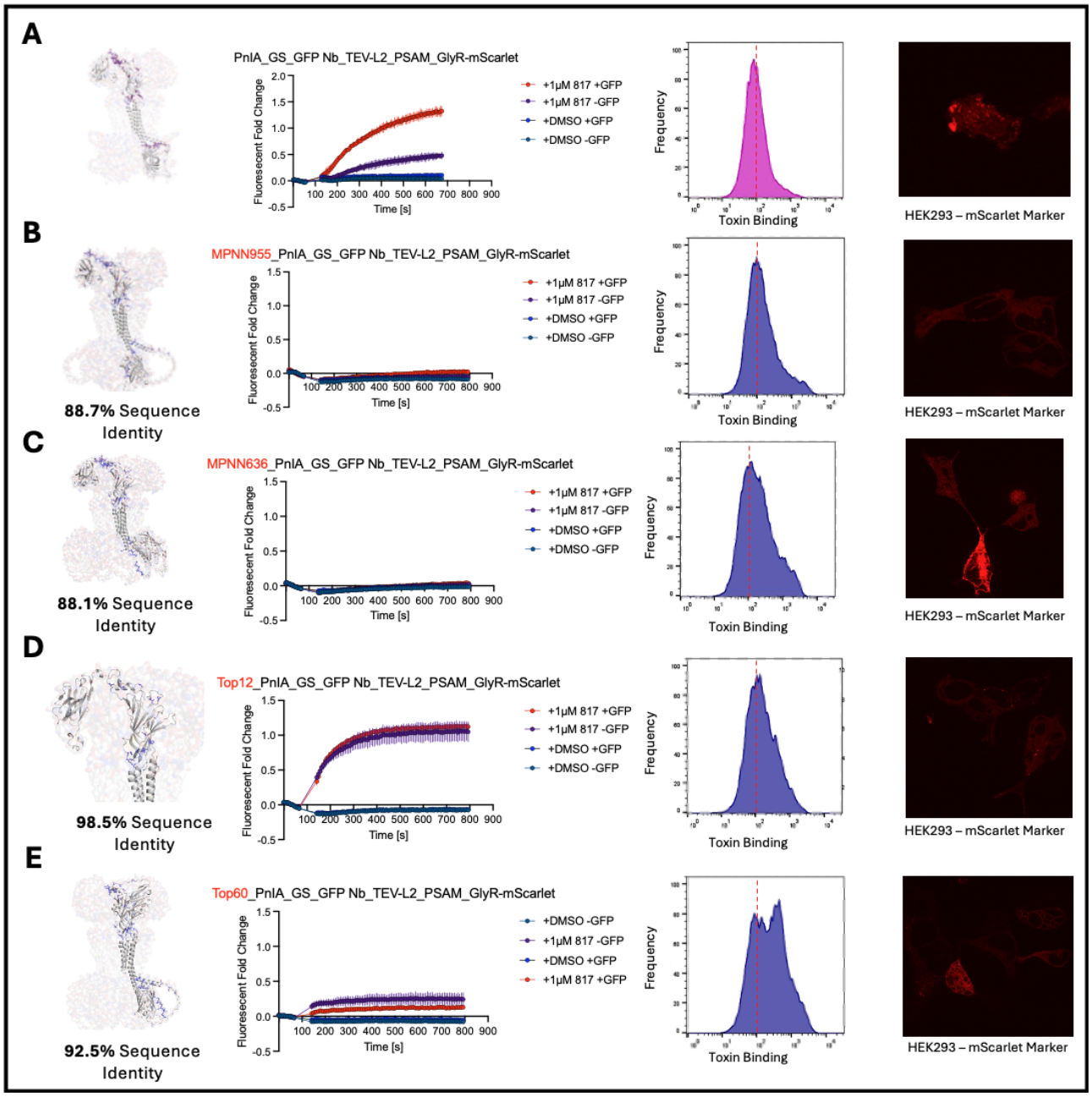

Figure 6. Experimental validation of ProteinMPNN-based backbone redesigns — due to time constraints, not all ordered sequences were evaluated. **A)** WT MAGIC structure with (future) mutated residues highlighted, MP assay results to demonstrate conductance; FACS results using fluorophore tagged α-bungarotoxin to investigate surface presentation; live-cell imaging using the internal mScarlet expression marker to examine trafficking qualitatively. **B, C)** Two full backbone redesigns by MPNN. Both showed LOF but marginally improved trafficking to the membrane. **D, E)** Incorporating the 12, 60 most prevalent mutations among the original 1024 generated, (from unique residues).

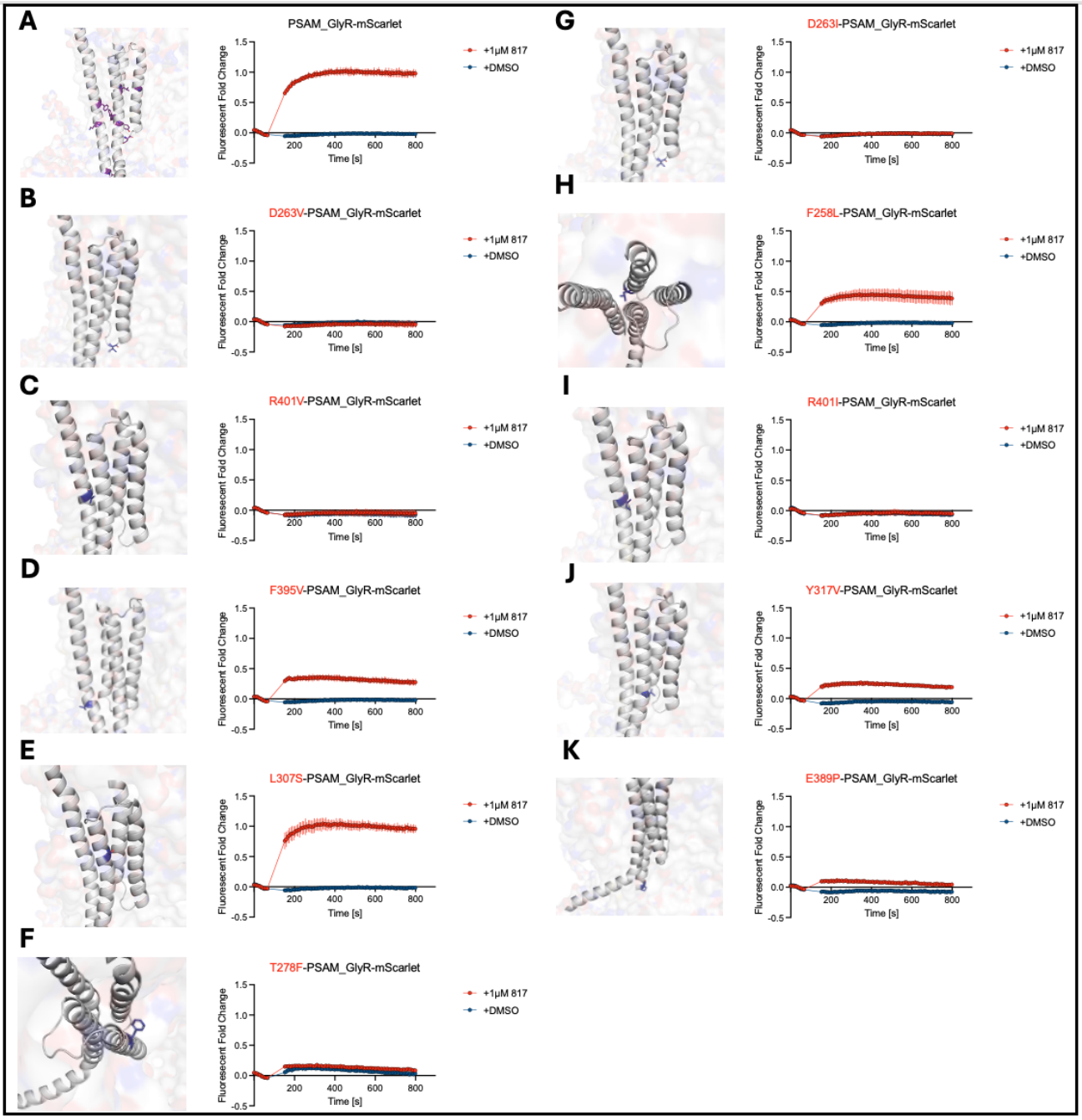

Figure 7. Experimental validation of CB-generated point mutants. **A)** WT, ungated MAGIC structure with (future) mutated residues highlighted, MP assay to test functional channel conductance. **B-K)** Structures and validating MP assay results for the top 10 predicted point mutants.